Journal of Geodesy (2001) 74: 720–729

Journal of Geodesy

Precise tidal gravity recorded with superconducting gravimeters at stations Wuhan (China) and Kyoto (Japan)

H.-P. Sun[1], S. Takemoto[2], H.-T. Hsu[1], T. Higashi[2], A. Mukai[3]

[1] Institute of Geodesy and Geophysics, Chinese Academy of Sciences, Xu-Dong Road 54, 430077 Wuhan, China
e-mail: heping@asch.whigg.ac.cn; Tel./Fax: +86 27 86783841
[2] Department of Geophysics, Graduate School, Kyoto University, Oiwakecho, Kitashirakawa, 606-8502, Kyoto, Japan
e-mail: takemoto@kugi.kyoto-u.ac.jp; Tel.: +81 75 7533911; Fax: +81 75 7533917
[3] Faculty of Law, Nara Sangyo University, 3-12-1 Tateno-Kita, Sango-cho, Ikoma, 636-0821 Nara, Japan
e-mail: mukai@nara-su.ac.jp; Tel.: +81 745 737800

Received: 20 January 2000 / Accepted: 15 September 2000

Abstract. Three long series of tidal gravity observations, totalizing approximately 24 years and recorded with three superconducting gravimeters, T004, T008, and T009, at stations Wuhan (China) and Kyoto (Japan), are studied. The tidal amplitude factors and phase differences are determined precisely using Eterna and Nsv techniques. The precision of the main tidal amplitudes is at the same level of 0.01 μGal. The atmospheric gravity signals are corrected using the coefficients determined with a regression method between tidal gravity residual and station air pressure. The oceanic gravity signals are modeled based on five global oceanic models. It is found that the oceanic models developed by the analysis of measurements from Topex/Poseidon altimeters have the best fit to the superconducting gravimeter measurements, since the observed residuals and the discrepancies between the amplitude factors and the theoretical tidal models are reduced more significantly. The long-period gravity variations are dominated by the non-linear drift phenomena of the instruments, and the short-term variations in gravity are due to the background noise at the stations.

Key words: Superconducting gravimeters – Tidal gravity – Pressure and oceanic gravity signals

1 Introduction

It is possible to study various problems in geophysics and geodynamics using tidal gravity observations recorded with modern Goodkind–Warburton–Reineman (GWR) superconducting gravimeters (SGs). It is extremely important to obtain long series of observations distributed worldwide, taking into consideration the fact that some valuable gravity signals with regional and global characteristics are quite weak. It is known that SGs have an extremely high sensitivity, with a precision of the order of 1 nanoGal (10^{-12} *g*) and a long-term stability at the level of approximately 1 μGal per year (Warbuton 1985; Goodkind 1991). SGs possess a wide measuring range, dynamic linearity and an extremely low noise level. They provide reliable measurements with which to determine the detailed structures of regional and global gravity changes.

The Global Geodynamics Project (GGP) started on 1 July 1997 with the participation of 18 SG stations around the world. The GGP will use tidal gravity data to study geodynamical problems, such as Earth tides, the nearly diurnal-free wobble and modes of the Earth's core, Earth's rotation and polar motion, interaction of the Earth with atmosphere and oceans, gravity changes due to tectonic motions, and so on (Crossley et al. 1999; Courtier et al. 2000).

This paper aims to summarize the results obtained in the Wuhan (China) and (Kyoto) Japan stations prior to the start of the GGP.

The Wuhan SG numbered T004 was installed in November 1985 on the ground floor of the main building of the Institute of Geodesy and Geophysics, Chinese Academy of Sciences in Wuhan (30.58°N, 114.36°E, 34 m). A main road at 60 m from the building and regular movements due to staff movements during working days produce high-frequency vibrations that increase the background noise. This kind of noise influences the precision of the tidal gravity parameters, i.e., tidal amplitude factors and phases. An analog record was used initially with the hourly readings measured manually. A digital data acquisition system was installed in November 1988. Data with 20-s intervals are decimated from the original 1-s sampling by a 22-bit digital recorder. The hourly tidal gravity data are decimated during the preprocessing procedure (Sun et al. 1998; Vauterin 1998). The atmospheric pressure records are obtained from the Wuhan base station included in the national meteorological network.

The Kyoto SGs, numbered T008 and T009, were installed in March 1988 on the concrete basement of the

Correspondence to: H.-P. Sun

ground floor in the main building of the Department of Geophysics, Kyoto University (Higashi 1996; Takemoto et al. 1998) (35.03°N, 135.79°E, 60 m), perpendicular to each other. The data acquisition system and compressors of the cryogenic refrigeration system were set up in the front room to avoid any disturbance caused by entering the observation room or the vibration of the compressors. Since the station is located in an urban area, the records are noisy, especially during the daytime. However, comparing observations of tidal gravity at the same station is very important to the study of the instrument characteristics. The data acquisition system consists of 24-bit digital recorders to ensure a wide dynamic range, and the atmospheric pressure is recorded with the same data acquisition system.

2 Data processing method

There are two filters, namely "TIDE" and "MODE", for the GWR SGs. The TIDE filter is a low-pass filter with a cut-off frequency around 50 s, while the MODE filter is a band-pass filter that is flat from 1 to 50 cycles per hour (Warbuton 1985). The hourly data are decimated from a 10-minute sampling of the TIDE filter. In order to convert the voltages to gravity values, the scale factor needs to be determined accurately. The scale factors were estimated from the amplitude factors obtained with the Lacoste–Romberg Earth Tidal (LCR-ET) model tidal gravimeters for T004 at Wuhan (Hsu et al. 1991, 2000) and from those recorded by the Askania GS-15 gravimeters for T008 and T009 at Kyoto (Higashi 1996).

The preprocessing procedure is carried out before the tidal analysis following standard procedures. Spikes and "offsets" of several μGal of unknown origin frequently occur. The abnormal signals are detected and eliminated by using a moving window function. Short-term gaps, due to power failures, earthquakes and liquid Helium refilling, are filled using a spline interpolation method based on a synthetic tidal gravity model reference at the station. The hourly tidal gravity and station air pressure data are decimated after the data smoothing process.

The tidal parameters (amplitude factors and phase differences) are determined using the Eterna (Wenzel 1997) and Nsv (Venedikov et al. 1997) software. As a first step, band-pass filtering is used to eliminate the instrumental drift and long-term change in gravity. Using complete tidal generating potential development (Tamura 1981), the so-called observation equations are constructed for long-period (LP), diurnal (D), semi-diurnal (SD), and ter-diurnal (TD) bands based on continuous, hourly data sets. These equations are then solved using the classic least-squares (LS) method, and the tidal parameters and the associated root-mean–square (RMS) errors are determined. The observed tidal residuals in the time domain are obtained by subtracting the synthetic tidal gravity signals at each station from the original observed ones. The coefficients between gravity and station air pressure are determined using a simple regression method in both the time and frequency domains. The RMS errors of the main waves are obtained by spectral analysis using the Fast Fourier Transform (FFT) technique.

3 Determination of the tidal parameters

The long series of tidal gravity observations and station air pressure are used to determine the tidal parameters. For T004, the data cover the period from 1 January 1986 to 31 December 1994; for T008, it is from 7 October 1990 to 1 November 1997; and for T009 from 17 August 1989 to 9 October 1998. The variations of the tidal parameters (tidal amplitude factors and phases) are obtained by using Eterna and Nsv software. It is found that the two methods provide very similar results. The disparity for the main tidal amplitude factors is less than 0.1% in the D and less than 0.2% in the SD. This difference may be caused by biases in the filtered gravity data due to the Gibbs effect when applying the band-pass filtering (Liu et al. 2000); however, it is at the present observational noise level.

Tables 1 and 2 show the analysis results when using Nsv, i.e., the tidal parameters and the corresponding

Table 1. Tidal amplitude factors in D, SD, and TD wave bands

Wave	T004 (Wuhan)		T008 (Kyoto)		T009 (Kyoto)	
	δ	$\pm\delta$	δ	$\pm\delta$	δ	$\pm\delta$
SIGQ	1.12435	0.05659	1.18635	0.03704	1.22062	0.03702
2Q1	1.17407	0.01671	1.20060	0.01146	1.22010	0.01113
SIG1	1.19792	0.01399	1.20195	0.00956	1.21690	0.00945
Q1	1.18487	0.00217	1.20813	0.00148	1.20808	0.00147
RO1	1.18122	0.01105	1.19685	0.00741	1.20829	0.00738
O1	1.17872	0.00040	1.20585	0.00027	1.20512	0.00026
TAU1	1.20708	0.03420	1.23222	0.01601	1.21829	0.01740
NO1	1.17578	0.00467	1.19985	0.00324	1.19834	0.00312
CHI1	1.17043	0.02518	1.21786	0.01712	1.17022	0.01667
PI1	1.19759	0.01516	1.19492	0.00845	1.18100	0.00872
P1	1.17016	0.00091	1.19442	0.00049	1.19517	0.00051
S1	1.46963	0.05534	1.42571	0.03001	1.39433	0.03135
K1	1.15140	0.00029	1.18365	0.00018	1.18344	0.00019
PSI1	1.34506	0.03694	1.30820	0.02090	1.34622	0.02143
PHI1	1.14282	0.02100	1.21845	0.01151	1.22899	0.01187
TETA	1.17430	0.02537	1.19608	0.01695	1.21178	0.01680
J1	1.17637	0.00484	1.19493	0.00323	1.19467	0.00315
SO1	1.14618	0.02877	1.15290	0.02059	1.15905	0.01962
OO1	1.16182	0.00684	1.18075	0.00712	1.18120	0.00577
NU1	1.14713	0.03618	1.15076	0.03666	1.17147	0.02975
EPS2	1.15956	0.02440	1.22211	0.02082	1.20798	0.02745
2N2	1.19045	0.00716	1.21243	0.00639	1.21157	0.00818
MU2	1.18695	0.00613	1.20855	0.00527	1.20458	0.00704
N2	1.17985	0.00095	1.19761	0.00082	1.19634	0.00109
NU2	1.17422	0.00485	1.19097	0.00412	1.19033	0.00550
M2	1.17617	0.00018	1.19821	0.00015	1.19796	0.00020
LAMB	1.20001	0.02299	1.20180	0.01932	1.20145	0.02600
L2	1.16857	0.00559	1.19081	0.00405	1.20236	0.00644
T2	1.17117	0.00598	1.20210	0.00536	1.19617	0.00700
S2	1.17310	0.00036	1.20161	0.00031	1.20087	0.00041
K2	1.16734	0.00116	1.20027	0.00131	1.20276	0.00158
ETA2	1.17650	0.01792	1.20824	0.02225	1.20927	0.02480
2K2	1.17495	0.04929	1.16456	0.09645	1.19008	0.08690
MN3	1.01915	0.01394	1.06696	0.00967	1.08620	0.00844
M3	1.07261	0.00366	1.08021	0.00248	1.07775	0.00220

RMS errors for 20 main D, 13 main SD and two main TD waves. These results are obtained after applying the station pressure correction using the frequency-dependent atmospheric gravity admittance (see Table 4). The precision of the main wave amplitudes in the D, SD, and TD from three instruments is at the same level of 0.01 μGal. It is found that the amplitude factors are much larger and phase difference less negative at Kyoto than are those obtained at Wuhan. It will be shown that this is mainly due to the influence of the Pacific oceanic tides. Compared to the results obtained from the European stations of Brussels and Strasbourg (Sun et al. 1998), the phase differences at stations in Asia show negative values. Sun et al. (1998) show that this is due to the different characteristics in oceanic tides for the Pacific and Atlantic oceans as well as to the regional crustal structures.

It is important to check standard deviations (Stdvs) obtained from harmonic analysis, since these are usually used to judge the quality of the original observations. The Stdvs at the various tidal wave bands have been investigated systematically using the Nsv method. After local air pressure correction, and in D, SD, and TD wave bands, the Stdvs are given as 1.866, 1.492, and 0.56 μGal (T004), 0.877, 0.920, and 0.269 μGal (T008), and 1.169, 1.553, and 0.297 μGal (T009). As the Stdvs are related to the station environment, this means that the noise level at Wuhan is higher than that at Kyoto. The amplitude factor of Ψ1, which has a frequency close to one sidereal day, is much higher. This is due to the resonance effect of the Earth's core.

The tidal parameters for the long-period tidal wave (MF) are analyzed and given in Table 3. It is found that after applying the pressure correction, the precision of tidal amplitude factors and phase differences is improved significantly. The relative precision of the amplitude factors is given as 3.3% (T004), 26.6% (T008), and 17.0% (T009). The amplitude factor obtained at the Wuhan station is close to the theoretical prediction. However, the results obtained from T008 and T009 at the Kyoto station are not identical; there exists a relatively large discrepancy. This may relate to the different instrumental characteristics, including the calibration of the amplitude factor and phase, and a further investigation will be carried out. The phases determined for the MF waves at Kyoto are not significant due to the large errors involved.

Table 2. Tidal phase differences in D, SD, and TD wave bands

Wave	T004 (Wuhan)		T008 (Kyoto)		T009 (Kyoto)	
	$\Delta\varphi$ (°)	$\pm\Delta\varphi$	$\Delta\varphi$ (°)	$\pm\Delta\varphi$	$\Delta\varphi$ (°)	$\pm\Delta\varphi$
SIGQ	1.9968	2.8910	1.0791	1.8038	2.7403	1.7414
2Q1	0.8686	0.8160	1.7917	0.5453	1.3520	0.5222
SIG1	0.7792	0.6676	1.4187	0.4552	1.5031	0.4445
Q1	−0.2848	0.1045	0.8944	0.0703	0.9493	0.0694
RO1	−0.5854	0.5351	0.4808	0.3541	1.1284	0.3493
O1	−0.5790	0.0193	0.2925	0.0127	0.3413	0.0125
TAU1	−1.3212	1.6224	1.2907	0.7438	0.7545	0.8178
NO1	−0.5494	0.2278	−0.1040	0.1546	−0.0209	0.1493
CHI1	−2.9177	1.2324	−1.4509	0.8059	−0.2653	0.8164
PI1	−0.9006	0.7264	−0.0209	0.4058	−1.4341	0.4229
P1	−0.8221	0.0442	−0.4664	0.0238	−0.3774	0.0246
S1	−29.053	2.1577	12.2847	1.4298	15.8971	1.5442
K1	−0.7300	0.0147	−0.5381	0.0090	−0.4801	0.0090
PSI1	2.1371	1.5722	−3.2719	0.9168	−3.2776	0.9122
PHI1	−0.9070	1.0537	1.0470	0.5422	−1.6388	0.5532
TETA	−0.9563	1.2386	0.1507	0.8118	−0.7121	0.7939
J1	−0.8648	0.2359	−1.4096	0.1545	−1.3914	0.1510
SO1	−1.7764	1.4381	−2.7181	1.0226	−1.8155	0.9718
OO1	−1.0627	0.3375	−2.3238	0.3455	−1.7511	0.2803
NU1	0.2882	1.8055	−1.4849	1.8231	−3.0486	1.4570
EPS2	−0.7603	1.2058	0.0712	0.9789	0.1691	1.3051
2N2	−0.6484	0.3446	−0.3950	0.3023	−0.3491	0.3870
MU2	−0.1099	0.2959	−0.2117	0.2501	−0.1542	0.3351
N2	−0.6616	0.0460	−0.4753	0.0395	−0.2315	0.0524
NU2	−0.7815	0.2366	−0.6719	0.1982	−0.4382	0.2649
M2	−0.6307	0.0086	−0.1934	0.0072	−0.0832	0.0098
LAMB	−0.9424	1.0981	−1.5112	0.9189	−2.8048	1.2368
L2	0.0233	0.2745	−0.2511	0.1950	−0.4732	0.3066
T2	−1.7424	0.3373	−1.2823	0.2634	−1.2985	0.3377
S2	−0.5753	0.0174	−0.6856	0.0152	−0.5645	0.0201
K2	−0.5552	0.0554	−0.7057	0.0629	−0.6848	0.0751
ETA2	−1.6632	0.8740	0.3518	1.0552	−0.9545	1.1751
2K2	−0.1865	2.4034	−2.5284	4.7435	−0.8237	4.1854
MN3	1.3468	0.7850	−1.2267	0.5194	−0.3491	0.4454
M3	−0.1959	0.1959	−0.2439	0.1318	−0.0813	0.1172

4 Atmospheric gravity signals

The influence of the atmospheric pressure on and tidal gravity recording cannot be neglected (Sun 1995; Sun et al. 1995). A strong correlation between tidal residuals and changes in station pressure is found at the Wuhan and Kyoto stations. In order to eliminate pressure influence prior to the determination of the tidal

Table 3. Tidal amplitude factors for the MF wave

Model	δ ($\pm\delta$)	$\Delta\varphi$ ($\pm\Delta\varphi$) (°)
T004	1.16338 (±0.03829)	1.8467 (±1.9258)
T008	1.05125 (±0.27925)	0.3748 (±15.0286)
T009	1.77512 (±0.30200)	6.8431 (±10.0329)

Table 4. Atmospheric gravity regression coefficients

Wave	T004 (Wuhan)		T008 (Kyoto)		T009 (Kyoto)	
	μGal/hPa	RMS	μGal/hPa	RMS	μGal/hPa	RMS
LP	−0.3780	±0.0199	−0.3534	±0.0130	−0.3332	±0.0151
D	−0.3000	±0.0198	−0.3510	±0.0070	−0.3462	±0.0069
SD	−0.1990	±0.0398	−0.3564	±0.0279	−0.2611	±0.0363
TD	−0.1467	±0.0171	−0.2753	±0.0096	−0.2354	±0.0081

Table 5. Tidal residuals before and after oceanic loading correction (T004, Wuhan)

Wave	Observed		Schwiderski		CSR3.0		FES95		ORI		ORI96	
	B (μGal)	β (°)	X (μGal)	χ (°)	X (μGal)	χ (°)	X (μGal)	χ (°)	X (μGal)	χ (°)	X (μGal)	χ (°)
Q1	0.165	−10.73	0.037	−30.27	0.029	−7.55	0.058	−32.80	0.052	52.88	0.030	−7.68
O1	0.750	−25.57	0.139	−62.03	0.124	−55.81	0.155	−51.13	0.119	−38.81	0.149	−50.18
P1	0.342	−38.33	0.148	−36.64	0.120	−28.96	0.104	−33.32	0.100	−28.64	0.134	−41.18
K1	0.842	−41.78	0.252	−64.51	0.185	−28.37	0.145	−43.63	0.149	−47.78	0.210	−54.92
N2	0.233	−38.46	0.117	−71.90	0.090	−78.93	0.052	−33.38	0.168	−100.4	0.094	−72.61
M2	1.040	−43.85	0.648	−72.36	0.513	−63.29	0.297	−1.17	0.676	−107.3	0.449	−77.95
S2	0.407	−48.50	0.272	−80.97	0.211	−82.31	0.164	−25.70	0.192	−116.6	0.196	−75.48
K2	0.086	−67.59	0.086	−122.1	0.066	−124.9	0.030	−137.7	0.089	−129.4	0.055	−117.6

Table 6. Tidal residuals before and after oceanic loading correction (T008, Kyoto)

Wave	Observed		Schwiderski		CSR3.0		FES95		ORI		ORI96	
	B (μGal)	β (°)	X (μGal)	χ (°)	X (μGal)	χ (°)	X (μGal)	χ (°)	X (μGal)	χ (°)	X (μGal)	χ (°)
Q1	0.321	19.19	0.023	−144.29	0.015	162.34	0.054	−52.57	0.093	64.00	0.022	87.51
O1	1.529	6.75	0.233	−130.14	0.221	−149.42	0.168	−122.49	0.175	−86.78	0.144	−109.28
P1	0.633	−12.03	0.058	−107.18	0.100	−149.04	0.086	−144.46	0.014	−176.69	0.083	−108.55
K1	2.058	−12.81	0.241	−111.08	0.187	−117.25	0.187	−100.30	0.365	−103.97	0.223	−86.35
N2	0.350	−15.88	0.114	−130.07	0.156	−124.00	0.091	−114.21	0.254	−133.22	0.144	−104.78
M2	1.801	−6.49	0.702	−123.74	0.741	−133.35	0.432	−109.66	0.789	−145.47	0.674	−120.16
S2	0.971	−20.30	0.190	−157.06	0.186	−146.53	0.059	−111.61	0.242	−159.54	0.162	−130.59
K2	0.257	−21.50	0.078	175.38	0.052	−162.89	0.043	−62.84	0.129	−142.28	0.048	−145.94

Table 7. Tidal residuals before and after oceanic loading correction (T009, Kyoto)

Wave	Observed		Schwiderski		CSR3.0		FES95		ORI		ORI96	
	B (μGal)	β (°)	X (μGal)	χ (°)	X (μGal)	χ (°)	X (μGal)	χ (°)	X (μGal)	χ (°)	X (μGal)	χ (°)
Q1	0.322	20.30	0.021	−159.67	0.019	143.50	0.048	−48.25	0.098	65.85	0.029	88.81
O1	1.512	7.96	0.227	−139.18	0.227	−158.69	0.158	−134.95	0.145	−94.63	0.127	−123.02
P1	0.639	−9.63	0.031	−102.55	0.080	−160.70	0.064	−157.40	0.025	99.01	0.056	−106.68
K1	2.039	−11.51	0.200	−118.36	0.150	−128.74	0.141	−107.15	0.319	−107.53	0.173	−88.01
N2	0.328	−8.17	0.093	−155.98	0.127	−141.10	0.059	−145.69	0.230	−143.85	0.103	−118.35
M2	1.780	−2.82	0.617	−130.69	0.671	−140.94	0.331	−118.46	0.740	−153.44	0.584	−126.94
S2	0.936	−17.22	0.192	−175.69	0.177	−165.99	0.039	173.50	0.245	−174.15	0.137	−152.62
K2	0.271	−19.76	0.062	171.82	0.036	−159.38	0.051	−45.28	0.115	−138.45	0.034	−134.66

Table 8. Tidal parameters before and after oceanic loading correction (T004, Wuhan)

Wave	Observed		Schwiderski		CSR3.0		FES95		ORI		ORI96	
	δ	$\Delta\varphi$ (°)	δ'	$\Delta\varphi'$ (°)	δ'	$\Delta\varphi'$ (°)	δ'	$\Delta\varphi'$ (°)	δ'	$\Delta\varphi'$ (°)	δ'	$\Delta\varphi'$ (°)
Q1	1.1849	−0.28	1.1611	−0.21	1.1603	−0.04	1.1649	−0.35	1.1610	0.47	1.1605	−0.04
O1	1.1787	−0.58	1.1566	−0.26	1.1568	−0.22	1.1580	−0.26	1.1578	−0.16	1.1579	−0.25
P1	1.1702	−0.82	1.1598	−0.40	1.1585	−0.27	1.1569	−0.26	1.1570	−0.22	1.1581	−0.40
K1	1.1514	−0.73	1.1382	−0.34	1.1398	−0.13	1.1381	−0.15	1.1379	−0.17	1.1385	−0.26
N2	1.1799	−0.66	1.1667	−0.61	1.1646	−0.48	1.1674	−0.15	1.1594	−0.91	1.1658	−0.49
M2	1.1762	−0.63	1.1668	−0.64	1.1675	−0.48	1.1689	−0.01	1.1584	−0.67	1.1646	−0.46
S2	1.1731	−0.58	1.1646	−0.60	1.1639	−0.47	1.1693	−0.16	1.1588	−0.38	1.1649	−0.42
K2	1.1673	−0.56	1.1551	−0.60	1.1564	−0.44	1.1589	−0.17	1.1533	−0.57	1.1584	−0.40

parameters, a regression method is used to determine the coefficients between tidal gravity residual and air pressure. The corresponding results for the LP, D, SD, and TD bands are given in Table 4. The average precision of the regression coefficients is given as 9.45% (T004), 4.31% (T008), and 5.65% (T009). These results fit well with those obtained at stations in Brussels and Strasbourg (Ducarme and van Ruymbeke 1990; Sun et al. 1998), in Potsdam (Neumeyer and Dittfeld 1997), and in Cantley (Merriam 1992). However, in the SD

Table 9. Tidal parameters before and after oceanic loading correction (T008, Kyoto)

Wave	Observed		Schwiderski		CSR3.0		FES95		ORI		ORI96	
	δ	$\Delta\varphi$ (°)	δ'	$\Delta\varphi'$ (°)	δ'	$\Delta\varphi'$ (°)	δ'	$\Delta\varphi'$ (°)	δ'	$\Delta\varphi'$ (°)	δ'	$\Delta\varphi'$ (°)
Q1	1.2081	0.89	1.1497	−0.15	1.1506	0.05	1.1609	−0.45	1.1627	0.89	1.1540	0.24
O1	1.2058	0.29	1.1476	−0.37	1.1459	−0.23	1.1501	−0.29	1.1542	−0.36	1.1518	−0.28
P1	1.1944	−0.47	1.1473	−0.24	1.1412	−0.23	1.1426	−0.22	1.1475	0.00	1.1465	−0.35
K1	1.1836	−0.54	1.1322	−0.33	1.1323	−0.24	1.1338	−0.27	1.1322	−0.52	1.1351	−0.32
N2	1.1976	−0.47	1.1536	−0.54	1.1519	−0.80	1.1581	−0.51	1.1413	−1.15	1.1582	−0.86
M2	1.1982	−0.19	1.1534	−0.69	1.1506	−0.64	1.1592	−0.48	1.1472	−0.53	1.1547	−0.69
S2	1.2016	−0.68	1.1537	−0.19	1.1547	−0.26	1.1615	−0.14	1.1510	−0.22	1.1573	−0.31
K2	1.2003	−0.71	1.1480	0.06	1.1533	−0.14	1.1664	−0.36	1.1436	−0.74	1.1551	−0.25

Table 10. Tidal parameters before and after oceanic loading correction (T009, Kyoto)

Wave	Observed		Schwiderski		CSR3.0		FES95		ORI		ORI96	
	δ	$\Delta\varphi$ (°)	δ'	$\Delta\varphi'$ (°)	δ'	$\Delta\varphi'$ (°)	δ'	$\Delta\varphi'$ (°)	δ'	$\Delta\varphi'$ (°)	δ'	$\Delta\varphi'$ (°)
Q1	1.2081	0.95	1.1496	−0.08	1.1505	0.12	1.1608	−0.39	1.1627	0.96	1.1539	0.31
O1	1.2051	0.33	1.1467	−0.31	1.1450	−0.17	1.1492	−0.23	1.1533	−0.30	1.1509	−0.22
P1	1.1952	−0.38	1.1482	−0.13	1.1421	−0.12	1.1435	−0.11	1.1484	0.11	1.1474	−0.24
K1	1.1834	−0.48	1.1320	−0.26	1.1320	−0.17	1.1335	−0.20	1.1320	−0.44	1.1349	−0.25
N2	1.1963	−0.23	1.1521	−0.23	1.1504	−0.49	1.1566	−0.21	1.1397	−0.85	1.1566	−0.56
M2	1.1979	−0.08	1.1531	−0.55	1.1503	−0.50	1.1589	−0.34	1.1469	−0.39	1.1544	−0.55
S2	1.2009	−0.56	1.1528	−0.04	1.1538	−0.11	1.1607	0.01	1.1502	−0.06	1.1564	−0.16
K2	1.2028	−0.68	1.1510	0.08	1.1563	−0.12	1.1694	−0.33	1.1465	−0.72	1.1581	−0.23

Table 11. Oceanic loading corrections for smaller tidal waves (residuals)

Wave	T004 (Wuhan)				T008 (Kyoto)				T009 (Kyoto)			
	Observed		Corrected		Observed		Corrected		Observed		Corrected	
	B (μGal) β (°)		X (μGal) χ (°)		B (μGal) β (°)		X (μGal) χ (°)		B (μGal) β (°)		X (μGal) χ (°)	
SIGQ	0.010	127.46	0.029	172.26	0.008	34.56	0.050	−154.49	0.019	41.69	0.041	−160.06
RO1	0.030	−23.79	0.009	−77.25	0.047	13.15	0.019	−145.46	0.063	23.68	0.005	136.29
NO1	0.054	−26.77	0.009	−20.16	0.107	−2.68	0.021	−147.23	0.103	−0.56	0.023	−160.68
PI1	0.038	−21.78	0.025	−15.56	0.035	−0.56	0.006	149.39	0.034	−44.28	0.026	−129.61
PSI1	0.028	32.87	0.026	45.71	0.027	−62.80	0.023	−112.93	0.035	−45.24	0.022	−81.34
PHI1	0.018	−145.93	0.022	−167.96	0.031	24.60	0.018	97.08	0.040	−30.84	0.016	−76.54
TETA	0.011	−48.02	0.007	−52.52	0.017	4.55	0.008	113.54	0.025	−15.28	0.003	−3.57
J1	0.057	−41.67	0.037	−41.42	0.111	−37.56	0.037	−122.37	0.110	−37.37	0.036	−123.85
OO1	0.026	−74.81	0.026	−73.30	0.067	−63.41	0.036	−127.63	0.055	−55.47	0.025	−147.01
2N2	0.043	−25.89	0.015	−53.01	0.064	−9.54	0.020	68.98	0.063	−8.59	0.020	73.08
MU2	0.042	−5.35	0.008	31.36	0.071	−5.56	0.023	82.46	0.065	−4.42	0.024	97.41
NU2	0.040	−54.34	0.027	−98.39	0.058	−26.32	0.038	−133.96	0.053	−18.23	0.034	−145.94
L2	0.009	4.57	0.005	148.47	0.041	−10.50	0.027	−153.54	0.058	−14.05	0.020	−112.37
T2	0.055	−77.33	0.052	−93.05	0.065	−34.49	0.026	−116.67	0.059	−39.22	0.031	−130.05

and TD wave bands, the coefficients at Wuhan are relatively low compared to those obtained from theoretical computation as of −0.36 μGal/hPa (Sun 1995). This reflects some special meteorological conditions on the Chinese continent, i.e., the main pressure contribution concentrates at the LP band. It may be also due to the temperature signals mixed in pressure records.

However, although the large atmospheric pressure variations are at period of days, the harmonic analysis indicates that the pressure energy concentrates mainly at S1 and S2 waves in D and SD tidal bands. After applying the corresponding air pressure correction, the tidal gravity amplitude factors are reduced and fit better, after oceanic loading correction, to those obtained from theoretical computation using Dehant–Defraigne–Wahr (DDW) standard tidal models (Dehant et al. 1998). Especially for the S2 wave, the amplitude factor is reduced by about 0.3%. The numerical results also show that after applying station pressure correction, in the D, SD, and TD bands, the Stdvs are reduced by about 3.6, 0.7 and 1.2% (T004), 24.8, 1.5, and 10.3% (T008), and 12.2, 1.3, and 3.0% (T009). This shows that the pressure correction in the D band is much more effective at Kyoto than at Wuhan.

Table 12. Oceanic loading corrections for smaller tidal waves (amplitude factors)

Wave	T004 (Wuhan)				T008 (Kyoto)				T009 (Kyoto)			
	Observed		Corrected		Observed		Corrected		Observed		Corrected	
	δ	$\Delta\varphi$ (°)	δ'	$\Delta\varphi'$ (°)	δ	$\Delta\varphi$ (°)	δ'	$\Delta\varphi'$ (°)	δ	$\Delta\varphi$ (°)	δ'	$\Delta\varphi'$ (°)
SIGQ	1.1244	2.00	0.9935	1.26	1.1864	1.08	0.9129	−7.47	1.2206	2.74	0.9412	−4.77
RO1	1.1812	−0.59	1.1563	−0.53	1.1968	0.48	1.1360	−0.62	1.2083	1.13	1.1494	0.21
NO1	1.1758	−0.55	1.1578	−0.08	1.1998	−0.10	1.1441	−0.30	1.1983	−0.02	1.1423	−0.20
PI1	1.1976	−0.90	1.1895	−0.52	1.1949	−0.02	1.1425	0.23	1.1810	−1.43	1.1261	−1.52
PSI1	1.3451	2.14	1.3509	3.56	1.3082	−3.27	1.2345	−3.97	1.3462	−3.86	1.2848	−4.06
PHI1	1.1428	−0.91	1.1240	−0.49	1.2185	1.05	1.1656	1.83	1.2290	−1.64	1.1780	−1.61
TETA	1.1743	−0.95	1.1680	−0.73	1.1961	0.15	1.1475	1.06	1.2118	−0.71	1.1661	−0.03
J1	1.1764	−0.86	1.1715	−0.65	1.1949	−1.41	1.1462	−0.81	1.1946	−1.39	1.1459	−0.78
OO1	1.1618	−1.06	1.1634	−1.22	1.1807	−2.32	1.1356	−1.34	1.1812	−1.75	1.1364	−0.64
2N2	1.1905	−0.65	1.1702	−0.49	1.2124	−0.39	1.1694	0.85	1.2116	−0.35	1.1684	0.91
MU2	1.1869	−0.11	1.1675	0.14	1.2086	−0.21	1.1651	0.86	1.2046	−0.15	1.1603	0.94
NU2	1.1742	−0.78	1.1605	−0.76	1.1910	−0.67	1.1454	−0.90	1.1903	−0.44	1.1447	−0.61
L2	1.1686	0.02	1.1594	0.10	1.1908	−0.25	1.1426	−0.50	1.2024	−0.47	1.1563	−0.78
T2	1.1712	−1.74	1.1612	−1.99	1.2021	−1.28	1.1526	−1.02	1.1962	−1.29	1.1455	−1.03

5 Oceanic gravity signals

The oceanic tidal gravity signals are the main perturbations on tidal gravity observations (Melchior 1994; Francis 1996). Therefore, it is vital to carefully remove these signals before using the tidal parameters in geophysics and geodynamics (Hinderer et al. 1990; Defraigne et al. 1994; Crossley et al. 1999; Xu et al. 1999; Courtier et al. 2000). In the early 1980s, the Schwiderski model provided the basic oceanic tidal data for the loading corrections. Previous studies show that the correlation between the predicted load vectors and the observed ones is up to 90% (Melchior and Francis 1996). Since 1992 the oceanic models have improved significantly due to the use of the Topex/Poseidon altimetric data and finite-element techniques. Therefore it is important to study the various oceanic models in order to select the one which best fits the tidal gravity observations in the Asian area.

The load vectors have been computed from five different global ocean models, each of them providing us with four main waves (Q1, O1, P1, and K1) in D and four main waves (N2, M2, S2, and K2) in SD. The global ocean models used in this study include the Schwiderski (Scw80), the most recent ones developed by the analysis of the precise measurements from the Topex/Poseidon altimeters, and those that result from parallel developments in numerical tidal modeling and data assimilation, such as the Csr3.0 (Eanes), Fes95 (Grenoble), Ori and Ori96 (Matsumoto) models. Analysis shows that the numbers of cells for the recent ocean models have increased from 41 236 (Scw80) to 176 792 (Csr3.0). The area covered has increased from 3.50×10^{14} (Scw80) to 3.61×10^{14} m^2 (Fes95). When including the inland oceans and lakes, it is increased to 3.71×10^{14} m^2 (Csr3.0). The resolution is also improved, from $1 \times 1°$ (Scw80) to $0.5 \times 0.5°$ (Csr3.0, Fes95, and Ori96). The latitude range is extended from −77.5°, 89.5° (Scw80) to −78.5°, 90.5° (Csr3.0), and to −85.0°, 89.5° (Fes95.2). The mean residual amplitude for

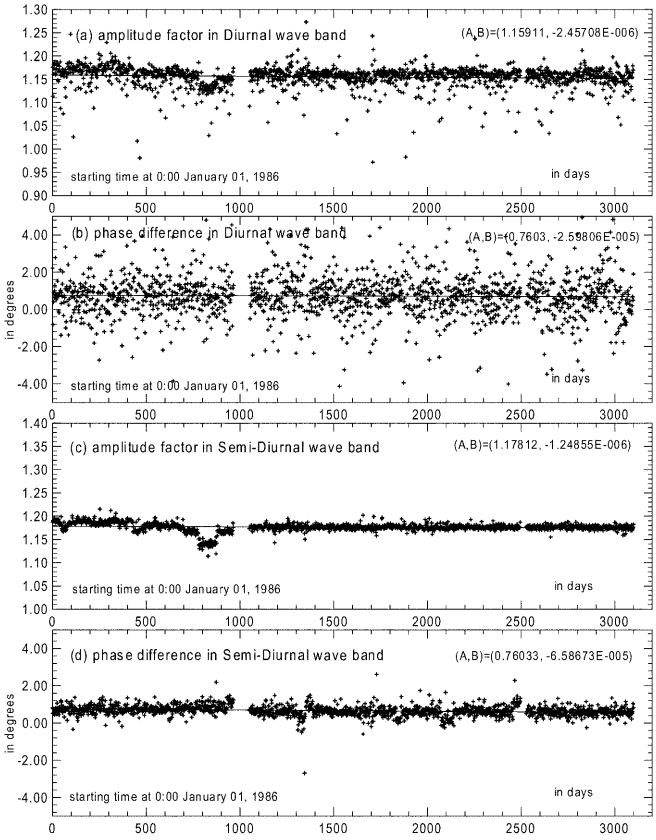

Fig. 1. Temporal variation of the tidal gravity factors and phase differences in D and SD wave bands for T004 (Wuhan)

M2 was reduced from 0.73 (Scw80) to 0.04 cm (Fes95.2), and to 0.02 cm (Csr3.0). This demonstrates that the recent ocean models cover a wider oceanic area, have higher resolution, and provide lower residual amplitudes.

For convenience, $\mathbf{L}(L, \lambda)$ is expressed as the load vector with amplitude L and phase λ. It includes the direct attraction of the periodic rise and fall of the ocean

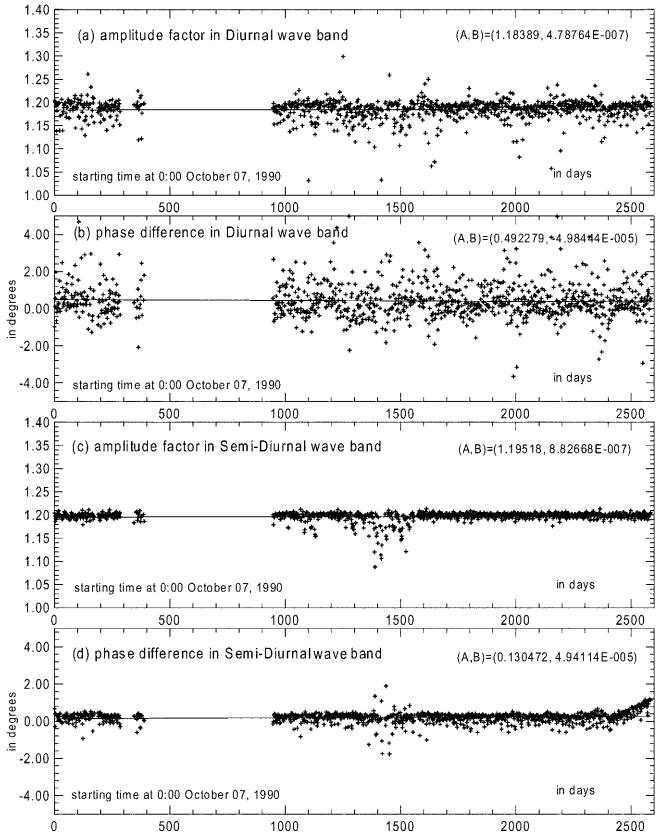

Fig. 2. Temporal variation of the tidal gravity factors and phase differences in D and SD wave bands for T008 (Kyoto)

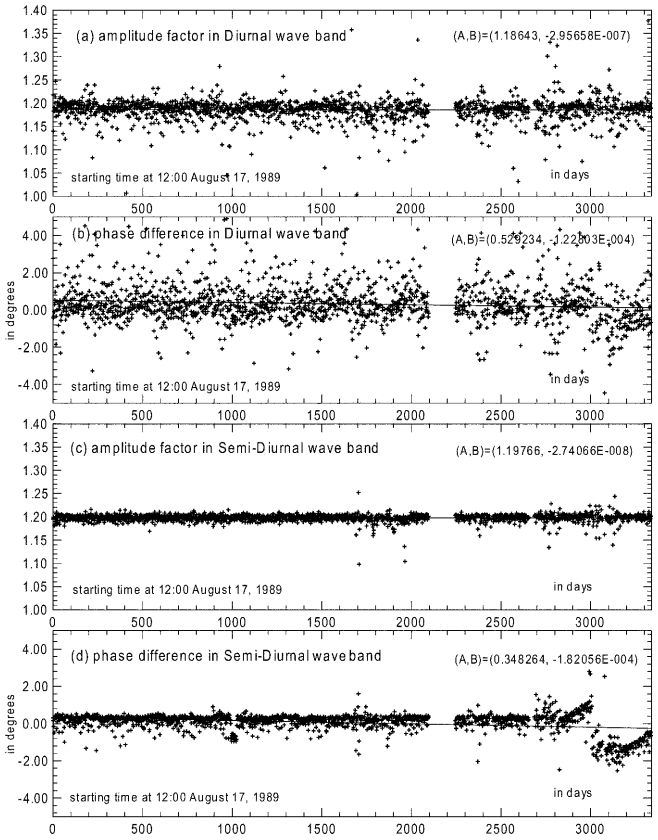

Fig. 3. Temporal variation of the tidal gravity factors and phase differences in D and SD wave bands for T009 (Kyoto)

water, as well as the loading contribution induced by the elastic deformation of the Earth. Based on the global ocean models and model Earth Green's functions (Farrell 1972), the influence of the ocean tides on gravity $\mathbf{L}(L, \lambda)$ is computed using a direct discrete convolution method (Sun 1992; Francis, pers. commun. 1997). It is found that the maximum oceanic gravity signal reaches at 0.6 μGal at Wuhan, and 2.0 μGal at Kyoto. The observed amplitude factor and phase difference are expressed as δ and $\Delta\varphi$, and those after ocean loading correction as δ' and $\Delta\varphi'$. The observed residuals $\mathbf{B}(B, \beta)$ with amplitude B and phase β are the difference between the observed tidal vector and the Earth tidal model. The smaller the B values are, the closer the model is to the observed values. It is found that the largest observed tidal residuals can reach 1.04 μGal (M2) for T004 (Table 5), 2.06 μGal (K1) for T008 (Table 6), and 2.04 μGal (K1) for T009 (Table 7). All other residual amplitudes are lower than 0.8 μGal at Wuhan and 1.8 μGal at Kyoto. The main difference between the real and the model Earth is that there exists a world ocean for the real one. Therefore, we can conclude that the tidal residuals are mainly due to the contribution of the oceans.

In order to check this theory, a second residual vector $\mathbf{X}(X, \chi)$, also called final residuals with amplitude X and phase χ, is introduced (Sun et al. 1999). It is obtained by subtracting the oceanic gravity signals **L** from the observed residuals **B** (Tables 5, 6, and 7). It is found that the observed residuals **B** are reduced significantly after the oceanic loading corrections. For the M2 wave of T004, **B** is reduced by about 38% (Scw80), 51% (Csr3.0), 71% (Fes95), 35%(Ori), and 57% (Ori96) μGal. For the K1 wave of T008, it is reduced by about 88% (Scw80), 91% (Csr3.0 and Fes95), 82% (Ori), and 89% (Ori96) μGal. For the M2 wave of T009, it is reduced by about 65% (Scw80), 62% (Csr3.0), 81% (Fes95), 58% (Ori), and 67% (Ori96) μGal. This means that the final residuals **X** are apparently reduced when applying the oceanic loading correction. It is found that the Grenoble (Fes95) and Matsumoto (Ori96) global oceanic models better fit the SG's measurements, since the final residuals are smaller than those obtained when using other models (Tables 5, 6, and 7).

Compared to the DDW theoretical tidal models (e.g. for Wuhan O1: 1.15377 and M2: 1.16262; and for Kyoto O1: 1.15379 and M2: 1.16265), the discrepancies between the observed amplitude factors (δ, $\Delta\phi$) and those after applying the loading correction (δ', $\Delta\phi'$) are reduced significantly (Tables 8, 9, and 10). For T004 and for the O1 wave, the discrepancies are reduced from 2.16% to 0.25% (Scw80), 0.26% (Csr3.0), 0.37% (Fes95), 0.35% (Ori), and 0.36% (Ori96), and for the M2 wave, from 1.17% to 0.36% (Scw80), 0.42% (Csr3.0), 0.54% (Fes95), 0.36% (Ori), and 0.17% (Ori96). For T008 and for the O1 wave, they are reduced from 4.51% to 0.54% (Scw80), 0.68% (Csr3.0), 0.32% (Fes95), 0.04% (Ori), and 0.17% (Ori96), and for the M2 wave, from 3.06% to 0.80% (Scw80), 1.04% (Csr3.0), 0.30% (Fes95), 1.33%

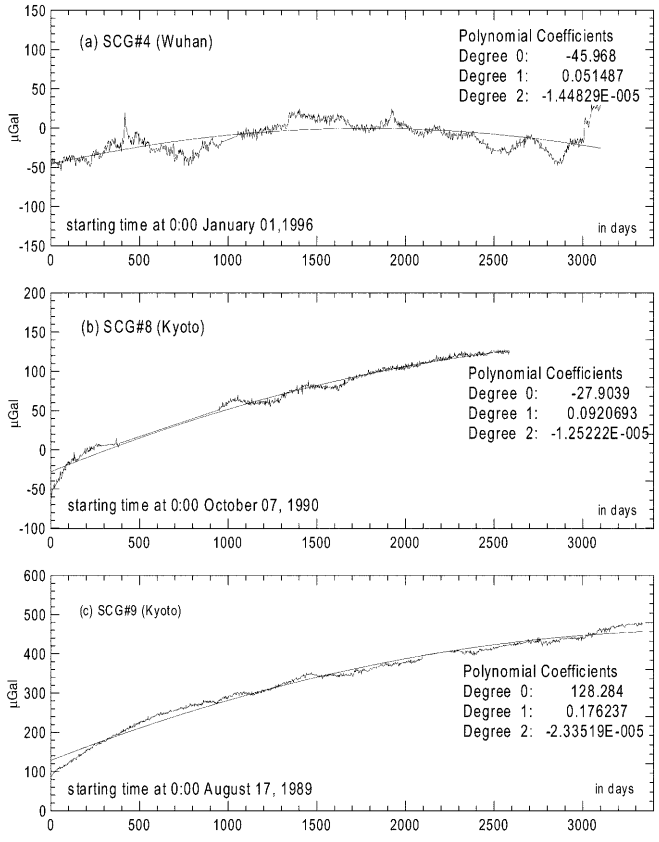

Fig. 4. Long-term temporal variation of the non-tidal gravity for T004, T008, and T009

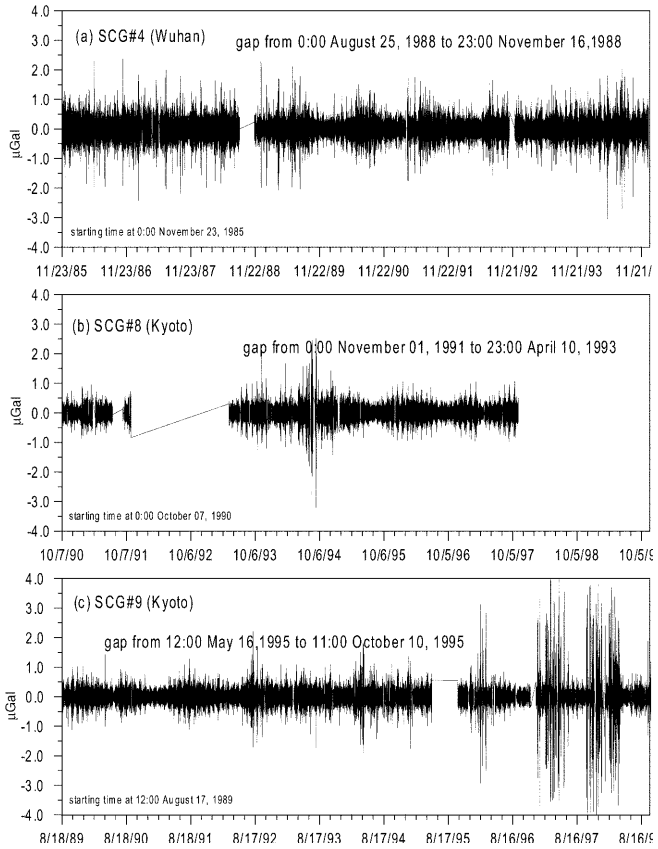

Fig. 5. Short-term, high-pass-filtered tidal gravity signals for T004, T008, and T009

(Ori), and 0.68% (Ori96). For T009 and for the O1 wave, they are reduced from 4.45% to 0.61% (Scw80), 0.76% (Csr3.0), 0.40% (Fes95), 0.04% (Ori), and 0.25% (Ori96), and for the M2 wave, from 3.03% to 0.82% (Scw80), 1.06% (Csr3.0), 0.32% (Fes95), 1.35% (Ori), and 0.71% (Ori96). The phase differences are also reduced at Wuhan; however, they are not effectively reduced at Kyoto. This may be due to the influence of the Japanese local oceanic tides since they are not yet included in the global models.

The present oceanic tidal models are not sufficient for some specific problems in geodynamics. For example, there are no ocean models at present for waves $\Psi 1$ and $\phi 1$ that have a frequency close to the free core nutation (FCN) resonance, i.e. one sidereal day. Based on the load vectors of eight main waves (Q1, O1, P1, K1, N2, M2, S2, and K2) computed from Schwiderski global ocean models and a second-order polynomial interpolation technique, the load vectors were obtained for 14 other waves.

Table 11 shows the tidal residuals before and after loading corrections for the 14 other smaller tidal waves. It is found that the observed residuals are reduced after loading correction. For the $\Psi 1$ wave, the residual is reduced by about 7.1% (T004), 14.8% (T008), and 37.1% (T009); for the $\phi 1$ wave, it is reduced by about 41.9% (T008) and 60.0% (T009) at Kyoto, but increased by about 18.2% (T004) at Wuhan. Table 12 shows the tidal amplitude and phases before and after oceanic loading corrections. It can be seen that the amplitude factors are improved to fit the DDW tidal predictions (e.g. for Wuhan $\Psi 1$: 1.26651 and $\phi 1$: 1.16943; and for Kyoto $\Psi 1$: 1.26770 and $\phi 1$: 1.16962). For the $\phi 1$ wave, the disparity is reduced from 0.4 to 0.1% (T004), from 4.1 to 0.34% (T008), and from 5.1 to 0.7% (T009). For the $\Psi 1$ wave, it is reduced from 6.2 to 1.3% (T009), but increased from 9.8 to 11% (T004) and from 3.2 to 10.5% (T008). It is found that the phase differences do not appear to be improved, which may be due to the influence of the complicated shallow oceanic tides along the coasts. A further study on this topic will be developed by using global SG measurements around the world under the scheme of the GGP.

6 Temporal change of the tidal parameters

In order to check the reliability of the data preprocessing, to show the stability of the instrument and to study the temporal characteristics of the Earth's response to tidal generating forces, the monthly results of the tidal parameters in D and SD bands are computed (Figs. 1–3). It is found that the wave amplitudes and phase differences are changed somewhat, especially after an interruption of the power supply or an instrumental adjustment. No apparent relation between these results and local geophysical phenomena, such as an earthquake event, is found. Compared to the temporal

changes in amplitude factors in the D band, it is found that in the SD band they are relatively stable. The scattering of the phase differences in the D band is relatively large, up to ± 1.5–$2.0°$. This may be due local or regional geophysical sources producing variations of the physical properties in the Earth's interior which lead to the variation of the Earth's response. Other influences should also be taken into account, such as regional air pressure changes, temperature variations, storms, and underground water changes.

7 Non-tidal gravity characteristics

Subtracting the synthetic tidal gravity signals at the stations from the original observed ones yields the non-tidal variations. Figure 4 shows the long-term apparent gravity changes for T004, T008, and T009. The drifts for T008 and T009 can be modeled by an exponential function (Mukai 1997). A jump appeared in October 1989 for T004, which is due to an instrumental adjustment (Fig. 4a) that also influenced the determination of the tidal parameters. It is found that the long-term tidal gravity variations are due mainly to the non-linear drift of the instruments. This may include the seasonal and yearly changes of underground water, regional air pressure, temperature changes, polar motion, and other unknown effects. The elimination of these perturbations is extremely important since they are probably not of tidal origin.

Figure 5 shows the short-term gravity signals after applying a high-pass filter with a cut-off of 0.5 cycles per day. It is found that the change in gravity at Wuhan is around ± 0.8 μGal, while it is around ± 0.5 μGal at Kyoto. These spurious signals are due mainly to the noise at the station, erroneous data, and other unknown causes. Attention should be paid to them since they can influence the accuracy of the determination of the tidal parameters.

8 Conclusions

Based on the above-mentioned procedures, results and discussions, it can be concluded that the precision of the main tidal wave amplitudes obtained at Wuhan, China and Kyoto, Japan are at the same level, i.e. 0.01 μGal. A strong correlation between tidal residuals and changes in pressure is found. The coefficients determined using a regression method between tidal gravity residual and station pressure are used to effectively correct the pressure influence. Oceanic loading corrections should be carried out before the tidal parameters are used to study problems in geodynamics. The Grenoble (Fes95) and the Matsumoto (Ori96) oceanic models fit the SG's measurements best, since the final residuals and the disparity with respect to the tidal models are smaller than those obtained when using other models. The long-term apparent gravity variations are mainly dominated by the non-linear drift phenomena of the instruments, and the short-term variations are mainly due to the background noise at the station. These should be eliminated for the precise determination of the tidal parameters and the application of the tidal results to problems in geodynamics.

Acknowledgements. This study is supported jointly by the National Nature Science Foundation of China (49925411, 49774223), the Chinese Academy of Sciences (KZ952-J1-411, KZCX2-106), and the Grant-in-Aid for Scientific Research from the Ministry of Education, Science and Culture of Japan (Grant 10041116). The SG's data acquisition system in Wuhan, China is supported by the Volkswagen Foundation (no. I/63542) via G. Jentzsch (University of Jena, Germany). H.-P. Sun also thanks the Japan Society for Promotion of Science (JSPS) for supporting to work in Kyoto University in 1999. B. Ducarme is greatly acknowledged for his suggestions on the interpolation of the oceanic load vectors, and for his constructive comments and careful correction to the manuscript. H.G. Wenzel and A.P. Venedikov provided their outstanding tidal analysis software.

References

Courtier N, Ducarme B, Goodkind J, Hinderer J, Imanishi Y, Seama, Sun HP, Merriam J, Bengert, Smylie DE (2000) Global superconducting gravimeter observations. Phy Earth Planet Int 117: 3–20

Crossley D, Hinderer J, Casula G, Francis O, Hsu HT, Imanishi Y, Jentzsch G, Kaananen J, Merriam J, Meurers B, Neumeyer J, Richter B, Shibuya K, Sato T, van Dam T (1999) Network of superconducting gravimeters benefits a number of disciplines. EOS. Trans Am Geophys Union 80(11): 121, 125–126

Defraigne D, Dehant V, Hinderer J (1994) Staking gravity tide measurements and nutation observations in order to determine the complex eigenfrequency of nearly free wobble. J Geophys Res 99(B5): 9203–9213

Dehant V, Defraigne P, Wahr JM (1998) Tides for an Earth in a non-hydrostatic equilibrium. In: Ducarme B, Paquet P (eds) Proc 13th Int Symp Earth Tides, Brussels, 20–24 July 1997, Série Géophysique. Royal Observatory of Belgium, Brussels, pp 261–263

Ducarme B, van Ruymbeke M (1990) On tidal parameters at Brussels fundamental station. In: Vieira R (ed) Proc 11th Int Symp Earth Tides, Helsinki, 1989. Schweizerbastische Verlagsbuchhandlung, Stuttgart, pp 157–166

Farrell WD (1972) Deformation of the Earth by surface loads. Rev Geophys 10: 761–779

Francis O (1996) Tidal loading in south Western Europe: a test area. Geophys Res Lett 23(17): 2251–2254

Goodkind JM (1991) The superconducting gravimeters: principals of operation, current performance and future prospects. In: Poitevin C (ed) Proc workshop on non-tidal gravity change. Conseil de l'Europe Cahiers du Centre Europeen de Geodynamics et de Seismologie, Luxembourg, vol 9, pp 81–90

Higashi T (1996) A study on characteristics of tidal gravity observations by employing superconducting gravity meters at Kyoto, Japan. Repr from memoirs of Kyoto University, Series of Physics, Astrophysics, Geophysics and Chemistry, A39(3): 313–348

Hinderer J, Zurn W, Legros H (1990) Interpretation of the strength of the ''nearly diurnal free wobble'' – resonance from stacked gravity tide observations. In: Vieira R (ed) Proc 11th Int Symp Earth Tides, Helsinki, 1989. Schweizerbastische Verlagsbuchhandlung, Stuttgart, pp 549–555

Hsu HT, Jahr T, Jentzsch G, Tao GX (1991) Some results from SCG in Wuhan/China. Bull Inf Marees Terrest 111: 7923–7979

Hsu HT, Sun HP, Xu JQ, Tao GX (2000) International tidal gravity reference values at Wuhan. Chin Sci Bull 43(1): 77–83

Liu LT, Xu HT, Sun HP, Hao XH (2000) Wavelet approach to the determination of gravity tidal parameters. Sci China (Series D) 43(2): 158–165

Melchior P (1994) A new data bank for tidal gravity measurements (DB92). Phys Earth Planet Int 82: 125–155
Melchior P, Francis O (1996) Comparison of recent ocean tide models using ground based tidal gravity measurements. Mar Geod 19: 291–330
Merriam JB (1992) Atmospheric pressure and gravity. Geophys J Int 109: 438–450
Mukai A (1997) Effect of the underground water on gravity observations at Kyoto. In: Segawa W, et al (eds) Proc Int Assoc Geod Symp, Gravity, geoid and marine geodesy, vol 117, Springer, Berlin Heidelberg New York, pp 123–130
Neumeyer J, Dittfeld HJ (1997) Results of the three year observation with superconducting gravimeter at the GeoForchungs Zentrum Potsdam. J Geod 71(2): 97–102
Sun HP (1992) Comprehensive researches for the effect of the ocean loading on gravity observations in the Pacific area. Bull Inf Marees Terrest 113: 8271–8292
Sun HP (1995) Static deformation and gravity changes at the Earth's surface due to the atmospheric pressure. Sér Géophys No Hors-Série. Royal Observatory of Belgium, Brussels
Sun HP, Ducarme B, Dehant V (1995) Effect of the atmospheric pressure on surface displacements. J Geod 70: 131–139
Sun HP, Ducarme B, Hindered J, Hsu HT (1998) Intercomparison of the (Non-)tidal gravity observations with superconducting gravimeters at stations Wuhan, Brussels and Strasbourg. In: Ducarme B, Paquet P (eds) Proc 13th Int Symp Earth Tides, Brussels, 20–24 July 1997, Série Géophysique. Royal Observatory of Belgium, Brussels, pp 453–462
Sun HP, Hsu HT, Luo SC, Xu JQ (1999) Study of the ocean models using tidal gravity observations obtained with superconducting gravimeter. (in Chinese with English abstract). Acta Geod Cartogr Sin 28(2): 115–120
Takemoto S, Dwipa S, Fukuda Y, Higashi T, Andan A (1998) Precise gravity observations in Bandung using a superconducting gravimeter. Paper presented to Symp Japan–Indonesia ID-NDR Project, August 1998, Bandung, Indonesia, pp 1–8
Tamura Y (1981) A harmonic development of the tidal generating potential. Bull Inf Marees Terrest 64: 677–704
Vauterin P (1998) Tsoft: graphical and interactive software for the analysis of Earth tide data. In: Ducarme B, Paquet P (eds) Proc 13th Int Symp Earth Tides, Brussels, 20–24 July 1997, Série Géophysique. Royal Observatory of Belgium, Brussels, pp 453–462
Venedikov AP, Vieira R, De Toro C, Arnoso J (1997) A new program developed in Madrid for tidal data processing. Bull Inf Marees Terrest 126: 9669–9682
Xu JQ, Hsu HT, Sun HP, Luo SC (1999) Investigation of the Earth's nearly diurnal free wobble resonance using tidal gravity observations with superconducting gravimeters (in Chinese with English abstract). Chin J Geophys 42(5): 599–608
Warbuton (1985) GWR instruments cryogenic refrigerating manual. San Diego, University of California
Wenzel HG (1997) The nanogal software: data processing package Eterna 3.3. Bull Inf Marees Terrest 124: 9425–9439